IJBPAS, June, 2024, 13(6): 2816-2836

ISSN: 2277–4998

International Journal of Biology, Pharmacy and Allied Sciences (IJBPAS)

'A Bridge Between Laboratory and Reader'

www.ijbpas.com

SYNTHESIS AND CHARACTERIZATION OF SILVER NANOPARTICLES WITH *PACHYGONE OVATA* (POIR.) LEAF EXTRACT AND EVALUATION OF ITS ANTICANCER EFFECT IN B16F10 AND FIBROBLAST (3T3) TUMOR CELLS

HARITHA KIRANMAI M[1], PAVANI Y[2], MURALI KRISHNA N[3] AND SUBBA RAO M[4*]

1: Research Scholar, Department of Chemistry, Acharya Nagarjuna University & Assistant professor, Department of Humanities and Sciences, GRIET (Gokaraju Rangaraju Institute of Engineering and Technology), Hyderabad-500090, Telangana, India

2: Assistant professor, Department of Freshman Engineering, P.V.P Siddhartha Institute of Technology, Kanuru-520007, Vijayawada, Andhra Pradesh, India

3: Assistant professor, Department of Chemistry V.R. Siddhartha Engineering College. Kanuru Vijayawada, Andhra Pradesh, India

4: Profesor, Department of Chemistry, Acharya Nagarjuna University, Nagarjuna Nagar-522510, Andhra Pradesh, India

***Corresponding Author: Dr. M. Subba Rao; E Mail: mannamsrao@gmail.com**

Received 15th April 2023; Revised 8th June 2023; Accepted 18th Sept. 2023; Available online 1st June 2024

https://doi.org/10.31032/IJBPAS/2024/13.6.8091

ABSTRACT

The present work is aimed to develop and characterize silver nanoparticles obtained by green synthesis from n- hexane leaf extract of *Pachygone ovata* (Poir.) and evaluate their cytotoxic potential in B16F10 cells and fibroblast (3T3) cell lines. In this study, AgNP morphology and size of the obtained nanoparticle were characterized by UV-visible (UV-vis) absorption spectroscopy, SEM-EDS for elemental composition and zeta potential (ZP), XPS and XRD analysis. The synthesized nanoparticles showed maximum absorbance at 420 nm according to UV–vis spectroscopy results at 24 hours' time. Silver nanoparticles and their quasi-spherical shapes were obtained with an average size of 19nm. Perform cell cycle analysis to elucidate the mechanism of cytotoxicity in B16F10 cells. The aqueous extract of *Pachygone ovata* (Poir.) Leaf extract was found to be effective in the environmentally friendly synthesis of silver

nanoparticles. Silver nanoparticles with spherical shapes, small sizes, and uniform properties were successfully synthesized. The nanoparticles produced had a significant impact on cell viability reduction. Metal nanoparticles are thought to have caused apoptosis, or cell death, in some cells.

Keywords: *Pachygone ovata* (Poir.) leaf extract, AgNPs, Characterization, MTT, B16F10 cells and fibroblast (3T3) cell lines, anti-cancer activity

1. INTRODUCTION

Cancer is a group of over 100 diseases characterised by uncontrolled cell growth as well as tissue and organ invasion. Cancer will kill 12.6 million people according to the WHO by 2030 **[1]**. Because of the EPR effect, nanoparticles (NPs) can deliver drugs to neoplastic cells and accumulate in tumour tissues. Reduced drug delivery to normal tissues improves chemotherapeutic pharmacokinetics. Metal nanoparticles kill cancer cells. These NPs interact with other molecules of interest and drugs due to their large reactive surface area and small size. As a result, they are superior to the others **[2]**. Metallic nanoparticles (MNPs) are less than 100 nm in size and can be created using simple, environmentally friendly methods. MNPs are created by combining functional metals. Catalysts, sensors, water treatment, clothing and cosmetic additives, and biomedical applications are all possible with NMs. AgNPs are being studied for their anti-diabetic, anti-malarial, anti-tumor, and anti-viral properties. These metals bind better to biomolecules and drugs **[3]**. Li *et al*. (2015) **[4]** synthesised and tested AgNPs functionalized with gallic acid against HeLa tumour cells and normal liver cells (HL-7702). Tumor cells were less viable as a result of ROS production. According to Castro-Aceituno *et al*. (2016) **[5]**, AgNPs decreased cell viability and increased reactive oxygen species in lung adenocarcinoma (A549), MCF7, and liver cancer (HepG2) cells. According to the literature **[6]**, free radicals increase reduced glutathione (GSH), ROS, and lipid peroxidation, which makes AgNPs antitumor. ROS increases DNA damage and apoptosis or necrosis **[7]**.

Nanoparticles can be made from root, leaf, bark, seed, flower, and fruit extracts **[7]**. Extracts are synthesised with silver salt solution. Color changes during AgNP formation. Centrifuge the mixture to collect AgNPs after synthesis. Nucleation and growth create AgNPs. Nucleation forms "clusters" of elemental silver (Ag_0) after Ag^+ ions are reduced. These are silver nanoparticles. AgNP suspensions have a yellow or brownish colour and a 400-450 nm UV light absorption band due to surface plasmon resonance. Although green synthesis is widely used in AgNPs synthesis,

toxic chemical reagents limit its biomedical use. Given this, Pachygone ovata is rarely used to synthesise AgNPs. So, this study synthesised, characterised, and tested the antiproliferative potential of nanoparticles made of silver nanoparticles (AgNPs) from *Pachygone ovata* (Poir.) plant extract.

2. MATERIALS AND METHODS

2.1 Plant material collection and authentication

The raw material for *Pachygone ovata (Poir.)* Miers ex Hook.f. & Thomson was authenticated by the Head Department of Botany at Acharya Nagarjuna University and was obtained from Tirupati in the Eastern Ghats of Andhra Pradesh in October 2018 **(Figure 1)**. The voucher for the herbarium is ANBH 121/2018. Before using the samples (leaf and stem parts), we allowed them to dry for a full month at room temperature in the shade.

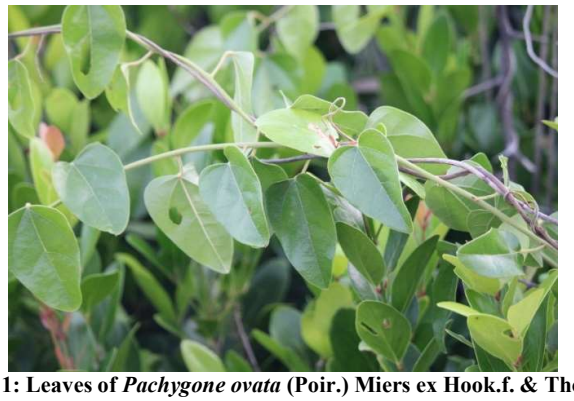

Figure 1: Leaves of *Pachygone ovata* (Poir.) Miers ex Hook.f. & Thomson

2.2 Preparation of Plant Extract

The plant leaf samples used within the scope of the study were thoroughly washed with tap water after species identification and left to dry at 50^{o}C for two days in an oven. Then, the grinding process was carried out with the help of a mortar and blender. 35 gr of ground plant sample was weighed and placed in a Soxhlet device containing 350 ml of n-hexane (Merck-India). It was extracted for 6-8 hours in the range of 30^{o}C to 60^{o}C. At the end of the period, a rotary evaporator at 37^{o}C was used to remove the extract dissolved in distilled water from the solvent. The extract, the solvent of which were separated, were stored in dark bottles at +4^{o}C degrees.

2.3 Green synthesis of silver nanoparticles

The methodology used for the synthesis of AgNPs in this work was based on that literature **[6]** the green synthesis process involves the reduction of silver by organic compounds, forming AgNP. 10 ml of the decomposed plant extract was taken and added into a flask. 90 ml of 1mM silver nitrate ($AgNO_3$) was placed on it. It was

stirred at 85°C (600 rpm) on a magnetic stirrer for 60minutes and the light brown to dark brown color change was considered as an indication of the conversion of silver ions to AgNPs. The colloidal suspension of the manufactured NPs (AgNP) was centrifuged (10,000 rpm, 4°C) for 15 minutes to complete the process, and the finished product was rinsed three times with deionized water to get rid of any unbound residues. The dried, purified AgNPs were then kept for future usage at 4°C in dark bottles after being dried in an oven for 15 hours at 50°C.

2.4 Physical-chemical characterization of silver nanoparticles

- **UV-visible spectroscopy:** This technique allows the detection of the presence of nanoparticles in suspension through characteristic light absorption. Readings between 350 and 600 nm were performed for nanoparticle suspensions using the PerkinElmer Lambda 2 Spectrometer. This allowed detecting the characteristic absorption range of nanoparticles for those synthesized with silver. This value is between 400 and 450 nm.
- **Scanning electron microscopy (SEM) analysis and Energy dispersive X-ray spectroscopy (EDS) analysis:** Scanning electron microscopy was used to observe the morphology of the synthesized AgNPs and also the size and distribution. Micrographs were obtained with Scanning Electron Microscope FEI-Quanta FEG 200F model. An elemental analysis was performed at a specific location on the membranes, using energy dispersive spectroscopy (EDS) coupled to SEM.
- **Transmission Electron Microscopy (TEM):** Using a JEOL – JEM – 2010F model equipment, samples washed with isooctane were examined on copper grids.
- **Fourier Transform Infrared Spectroscopy (FTIR):** For infrared spectroscopy (FTIR) analysis, 5 mg of the fraction and nanoparticles were pressed with the same amount of KBr forming a tablet, which was later analysed in a Shimadzu FTIR-8400S spectrometer. Thirty scans were performed for each sample in the range between 400 cm-1 and 4000 cm-1 at room temperature.
- **X-ray photoelectron spectrometer (XPS):** The silver nano material was studied using the XPS technique with a JEOL JPS-9200 X-ray photoelectron spectrometer to determine the binding energies of silver and to relate the functional groups associated with the silver nanoparticles. The equipment

uses a Mg Kα (hν = 1253.6 eV) X-ray source, operates at 10kV and 20mA (200W) and is equipped with a hemispherical electrostatic analyser with a mean radius of 100mm and a multichannel detector.

- **X-ray diffraction (XRD)** analysis is essential for the analysis of the phase and crystal structure of matter. The resulting NP powder was analyzed using an ADP PRO 2000 X-ray diffraction system with Cu Ka radiation (k = 1.54 A). The XRD pattern was studied with a step size of 0.02 in the range of 2θ between 10° and 80°. The crystalline area size was calculated using the Debye-Scherrer formula.

2.5 Cell lines

Normal 3T3 cells (Mouse embryonic fibroblast cells NIH/3T3 ATCC ® CRL-1658™) and B16F10 tumor cells (Mus musculus skin melanoma ATCC® CRL 6475™) cultured in Dulbecco's Modified Eagle Medium (DMEM) containing 10% (v /v) fetal bovine serum (FBS) and antibiotics (streptomycin and penicillin - 15 mg/L of medium). Cells were maintained under sterile conditions at 37°C with 5% CO_2 saturation.

2.5.1 Cell assays

Analysis of cell viability by the colorimetric method – MTT: This method evaluates the metabolic activity of cells by quantifying the reduction of MTT (3-(4,5-Dimethyl-thiazol-2-yl)-2,5-diphenyl-tetrazole bromide), by the action of mitochondrial dehydrogenases, by the formation of formazan crystals in cells with active metabolism **[7]**. To perform the MTT assays, the cells (B16F10 and 3T3) were plated in 96-well plates (5 x 10^3 cells per well) and left to rest for adhesion to the surface for 24 hours, in an oven at 37ºC with 5% CO_2 saturation. Subsequently, the culture medium was aspirated and, in its place, DMEM medium without fetal bovine serum was added to start the starvation process for a period of 24 hours. After this time, the medium was aspirated and in its place were added different concentrations of the 0.5v fraction (0.05, 0.5 and 1 mg/mL), AgNPs and silver nitrate (0.0025, 0.025 and 0.05 mg/mL) diluted in medium with fetal bovine serum for 24 hours. The concentrations shown for the AgNPs are taking into account the amount of silver quantified, so they are at 0.0025, 0.025 and 0.05 mg/mL. Subsequently, cell viability was determined by the colorimetric MTT test, through the addition of an MTT solution at 1 mg/mL for 4 h. After this period, the supernatant was removed and the formazan crystals were solubilized in ethanol. The plate remained under slow agitation for 15 minutes at room temperature, and the absorbance was measured at 570 nm in a microplate reader.

The results are presented in percentage of MTT reduction considering the absorbance of the negative control as 100% reduction.

Analysis of labeling of B16F10 cells with annexin V-FITC/propidium iodide: The Annexin V-FITC Apoptosis Detection Kit (Sigma-Aldrich, Inc. USA) was used for this experiment. The B16F10 cell line were transferred to 6-well plates ($2x10^5$ cells/well), the plates were incubated at 37 °C, with 5% CO_2 saturation for 24 hours **[8]**. After that time, the cells were deprived of medium without fetal bovine serum for 24 hours. Then, the culture medium was aspirated and the nanoparticles were applied at a concentration of 0.5 mg/mL with and without the caspase inhibitor ZVAD-FMK. Cisplatin was added to other wells at a concentration of 0.3 µg/mL for a positive control effect. After 24 h, the cells were trypsinized, collected and washed twice with phosphate buffered saline (PBS). Being centrifuged at 3200 rpm at 4°C for 5 minutes. The cells were washed, centrifuged twice more, and finally resuspended in 50 µL of the kit's buffer solution. Soon after, 5 µL of annexin-V and 1 µL of propidium iodide were added to the cells, being incubated for 30 min. After this period, 300 µL of binding buffer were added and the cell suspension was analyzed in a flow cytometer (Biosciences, San Diego, CA, USA). The percentage of cells undergoing apoptosis/necrosis was determined every 10,000 events and graphs represent data obtained from three separate experiments. For data analysis, the FlowJo® Analysis Software version 10.0.7 (Tree Star Incorporation, OR, USA) was used.

Cell cycle analysis: Cell cycle assessment of B16F10 cells was determined with the addition of propidium iodide (PI) **[9]**. PI is one of the dyes with affinity for DNA, it is capable of intercalating between small sequences of nucleotides and can only penetrate cells with damaged cell membranes. Cells of the B16F10 lineage were transferred to 6-well plates (2×10^5 cells/well), the plates were incubated at 37°C with 5% CO_2 saturation for 24 hours, being starved with medium free of fetal bovine serum. Then, the medium was aspirated and the nanoparticles were applied at 0.5 mg/mL. Cisplatin was added to other wells at a concentration of 0.3 µg/mL for a positive control effect. After the 24 h period, the cells were trypsinized, collected and washed twice with PBS. Being centrifuged at 3200 rpm at 4°C for 5 min. The cells were washed and centrifuged twice, resuspended in ice-cold 70% ethanol, and incubated at 4°C for at least 30 minutes. After incubation, each microtube was centrifuged at 3200 rpm for 5 minutes at 4°C. The supernatant was discarded and the samples were washed with 1x PBS and centrifuged again. After discarding the supernatant, 90 µL of Triton-

X and 10 µL of RNAse (4 mg/mL) were added to the pellet of each tube. Then, 5 µL of PI (Sigma-Aldrich, Inc. USA) and 200 µL of 1X PBS were added to tubes protected from light. After this procedure, the cells were analyzed in a flow cytometer.

2.6 Statistical analyses

Standard deviation was used to express the data as mean. Analysis of variance was used to assess the three copies of the data (ANOVA). The post-hoc Tukey-Kramer test ($p<0.05$) was performed to identify significant variations between the examined samples.

3. RESULTS

3.1 Characterization of AgNPs

UV Visible spectroscopic analysis: With regard to the evaluation of AgNPs for a period of 24 hours **(Figure 2)**, it was possible to perceive by UV-Vis, the increase in absorbance over time, which is directly related to the formation of AgNPs stable, as well as a shift referring to the 412 nm SPR band at 30 minutes, 1 hour and 2 hours and 3-hour time at 415 nm and 420 nm within 24 hours. The same was obtained by Erjaee, Rajain and Nazifi (2017) **[10]**, who found values of 414 nm in 2 hours and an increase to 422 in 24 hours. Such shifts are called redshifts, that is, for longer wavelengths, which occur when there is an increase in particle size.

SEM-EDX analysis: The SEM analyses were performed in parallel with the EDS analyses, so both analyses make up this topic. The images obtained by the SEM technique are displayed in **Figure 3a**. It is possible to visualize AgNPs with an average diameter of 19.86 ± 3.4 nm; It can also be seen in **Figure 3a** that the AgNPs have a rounded shape and are not aggregated. Scanning electron microscopy was used to analyze silver nanoparticles' surface and cross-sectional morphology. **Figure 3b** shows the cross-section of the AgNPs, with an average size of less than 20 nm.

With the EDS detector present in the SEM, it was possible to analyse the surface of the nanoparticles and obtain information on the chemical elements present in it and their respective percentages. In **Figure 3c**. The EDS spectrum of the nanoparticles is observed, in which there are strong signals in the silver region, allowing us to confirm silver's presence in them. Similarly, the percentages of the elemental composition of the nanoparticles can be observed in the insert. The synthesized nanoparticles present 7.2% silver, an unrepresentative value due to the coating of the organic residue of the nanoparticles. Likewise, the percentage of carbon reported is 41.2%, due to the organic nature of the extract and the adhesive layer on which the nanoparticles were placed, which is made of carbon. In the same way, an oxygen percentage of 51.6% is obtained, which comes from the organic nature of the extract.

Transmission Electron Microscope (TEM) Analysis: Silver nanoparticles made from *P. ovata* leaf n-hexane extract are depicted in **Figure 4a** using an electron microscope. It is noted that nanoparticles of various sizes are forming that are nearly spherical. The nanoparticles were identified as silver using selected area electron diffraction **(Figure 4b)**, as they exhibit a diffraction pattern that matches the face-cantered cubic structure typical of silver. The points of the diffractogram's rings correspond to the separations between the planes (111), (200), (220), and (311) of the silver structure. The histogram and the nanoparticles obtained from the *P. ovata* leaf extract are depicted in **Figure 4c**. The polydispersity coefficient of the silver nanoparticles is 43.24 and their average size is 19.25 nm 4.84 nm.

FT IR Analysis: The FT-IR spectroscopic analysis was used to determine or detect the chemical species that are bound on the surface of the nanoparticles and in the same way to observe the interactions between the extract and the obtained nanoparticles. **Figure 4** shows the spectra of the plant extract, the synthesized nanoparticles. The spectrum of the n- hexane extract from *P. ovata* leaves is shown in Fig 4(left) allows to analyse the main functional groups corresponding to it. A low intensity band can be seen, corresponding to the tension of the C-H bond at 2924 cm^{-1}. A stretching band of the C=O bond, of medium intensity at 1605 cm^{-1}, as well as a band at 1374 cm-1, of low intensity, caused by the twisting of the N-H bond **[11]**.

The spectrum of the synthesized silver nanoparticles can be seen in **Figure 4** (right) presents a band of low intensity located at 2966 cm^{-1}, caused by the stretching frequency of the C-H bond, a band of stretching frequency of the C=O bond, of medium intensity, at 1604 cm^{-1}, and a band at 1375 cm^{-1}, due to the twisting of the N-H bonds, which is due to the overlap of two bands present in the spectrum of the extract, which allows evidencing the participation of secondary amides or primary amines in the reduction process. The possible chemical compounds responsible for the C-H twist, C=O twist and N-H twist were analysed in the spectra of Fig 4. Similar results obtained by Ramachandran, *et al*. (2015) **[12]**, when using extract from Piper beetle leaves to synthesize silver nanoparticles and characterize them by FT-IR. With the results obtained, the main functional groups in the leaf extract are organic compounds **[13]**, which are responsible for the reduction thanks to the carbonyl groups in its structure.

Zeta potential of AgNPs by DLS: AgNPs synthesised from the *P. ovata* leaf extract had the parameters of size (nm), and zeta potential evaluated using the dynamic light scattering technique (DLS) **(Figure 5)**. The results obtained are displayed in **Table 1**. It

is observed for the AgNPs values of 19.6 ± 9 nm, these values are statistically different from each other. The zeta potential values measured were -25.9 mV for AgNPs.

3.2 Stability analysis of nanoparticles

The stability analyses of the nanoparticles occurred through the evaluation of the average diameter of the AgNPs by the DLS technique, for four months. The results are shown in **Figure 6**. During this period, a variation in the diameter was observed between the months tested, after this period the AgNPs probably aggregated and it was not possible to measure it. It is possible to notice that the diameter increased in the period between the first day and the 30th day of analysis. With subsequent measurements, it was observed that the average diameter of the nanoparticles tended to be smaller than that observed on the thirtieth day, but this decrease was not significant. On the 4th month (120days), the average diameter value of the AgNPs was significantly smaller compared to the previously measured values.

Finally, the nanocomposite was analysed by XPS to determine the binding energies of the reduced silver. **Figure 7 (a)** shows the complete spectrum where the signals of silver, oxygen and carbon are observed. To determine the oxidation states in which silver was present, a high-resolution XPS analysis was performed on the silver area. **Figure 7 (b)** shows the XPS spectrum of silver, where it can be seen that when performing a deconvolution of the $3d_{5/2}$ zone, it was found that silver presents two binding energies corresponding to metallic silver (Ag^0) and a complex formed with oxygen (Ag-O), which confirms the effectiveness of the reduction method proposed for the formation of silver nanoparticles from silver ions (Ag^{+1}) using *P. ovata* leaf extract as a reducing agent.

XRD (X-Ray Diffraction) was used to analyse the size, phase identification and crystal structure of AgNPs synthesized by the green synthesis method from *P. ovata* leaf extract. The XRD spectrum of the prepared AgNPs is at 2θ = 38.42, 44.63, 64.97, 78.15 for AgNP with characteristic Bragg diffraction schemes (111), (200), (220) and (310) of the face-centered cube. The Joint Committee on Powder Diffraction Standards (JCPDS) file no: 04-0781 database includes, respectively, the crystal structure of silver[21] **(Figure 8)**. The Scherrer formula, in which the average crystal size calculation is made with these diffraction peaks revealed in the XRD analysis, is given below. Using the Scherrer formula, the full width of the Ag (200) diffraction peak was taken into account, and the crystal size of Ag nanoparticles was 17.75, respectively.

$d(\text{Å}) = k\lambda / \beta cos\theta$

d = average size of NPs,

k= coefficient (0.9),

λ= X-ray wavelength (1,54056Å),

β = half-maximum point (rad) of the full width of the corresponding refractive peak, θ= denotes the angle of the peak at maximum height (rad).

3.3 Evaluation of the ability to reduce MTT

In this case, B16F10 and 3T3 strains were treated with AgNPs and silver from silver nitrate to evaluate these samples' influence on the cells' ability to reduce MTT after 24 hours of incubation. The results obtained are shown in **Figure 9**.

Cells from the murine fibroblastic lineage 3T3 were able to reduce the MTT affected by all tested samples, however, when viewing **Figure 9a**, a dose-dependent effect can be observed for AgNPs, in addition to an absence of this effect. effect when cells are treated with silver. On the other hand, there was a decrease of approximately 50% in the MTT reducing capacity of cells when they were treated with concentrations of 0.025 mg/mL and 0.05 mg/mL of AgNPs or silver. The influence of the samples on the murine melanoma lineage (B16F10) was also evaluated to observe the specificity of the nanoparticles for tumor cells. As seen in **Figure 9b**, none of the tested concentrations of silver influenced the ability to reduce MTT by B16F10 cells in a statistically significant way ($p<0.05$). At the lowest concentration (0.0025 mg/mL), the AgNPs did not influence the reducing capacity of MTT. With the other two concentrations (0.025 mg/mL and 0.05 mg/mL) it is possible to observe a dose-dependent effect of AgNPs on the MTT reduction capacity of these cells, as there was a decrease of 30% and 50%, respectively, in this capacity. The concentration of 0.025 mg/mL of AgNPs can be highlighted, as with this it was possible to influence the MTT reduction capacity of the tumor lineage. This did not occur with the standard strain (3T3), while silver in none of the tested concentrations, influenced the ability to reduce tumor cells.

3.6 Effects of AgNPs on B16F10 cells

Morphology of B16F10 tumor cells treated with AgNPs: To perform this analysis, B16F10 cells were exposed to AgNPs at a concentration of 0.5 mg/mL for 24 hours and then observed under an inverted phase-contrast microscope. As a negative control, only DMEM medium with FBS was used and as a positive control, cisplatin (0.3 µg/mL) was used, the images obtained are shown in Fig 10. Negative control cells **(Figure 10A)** did not show any apparent change in shape, preserving the fusiform aspect characteristic of this lineage; moreover, they were adhered to the surface of the plate forming a confluent monolayer. In Fig 10B, it can be seen that after treatment with cisplatin, fewer adhered cells are seen, compared to what is seen in the negative control group **(Figure 10A)**. In addition, the cells have a more triangular shape and surface projections can also be seen in some cells such as filopodia and

lamellipodia, indicated by the white arrow. As can be seen in **Figure 10C**, after treatment with AgNPs, a smaller number of adhered cells is visualized, in addition, the cells assume a globular shape. In **Figure 10D**, which is an enlargement of an area of **Figure 10C**, this globular aspect of the cells can be better verified (white arrow) and it is also possible to observe granules in the cytoplasm (white arrowhead) of the cells.

Analysis of labeling of B16F10 cells with annexin V and propidium iodide (PI) by flow cytometry: B16F10 cells were exposed to AgNPs, cisplatin (positive control) and medium with FBS (negative control) for 24 hours. were analyzed by flow cytometry. In **Figure 11**, the graphs obtained by the flow cytometry technique are displayed, the results are in the form of a graph divided into four quadrants with two axes, the "X" axis represents the number and intensity of cell marking with annexin and the axis "Y" represents cells with propidium iodide. **Figure 11A** shows the cytometry data for B16F10 cells in the absence of treatment (negative control). As can be seen, about 99% of the cells were not labeled by annexin V and propidium iodide. On the other hand, in **Figure 11B** we have the data related to the treatment with cisplatin (positive control), it can be seen that almost all the cells (99.8%) were double-marked for annexin V-PI. **Figure 11C** shows the data related to exposing cells to AgNPs. It is possible to notice that most of the cells (~88%) were marked by the two fluorophores, similar to what was observed for cells exposed to cisplatin. This behavior does not change significantly when cells were treated with the AgNPs concomitantly with the caspase inhibitor ZVAD-FMK **(Figure 11D)**.

Cell cycle analysis: The distribution of B16F10 cells in different cell cycle phases after exposure to different conditions was also evaluated. In this case, also with the use of flow cytometry. Therefore, after 24 hours, the labeling assays with propidium iodide were performed to evaluate the cell cycle phases. The results obtained are shown in **Figure 12**. It is noted in **Figure 12** that the highest percentage of B16F10 cells in the negative control is found in the G0/G1 phase (60.93%).

Furthermore, no significant difference was noticed between the percentages related to the S and G2/M phases (15.2% and 14.1%, respectively). It was also observed that there is a small percentage of particles labeled with iodide in Sub-G1 (9.77%). When analysing the positive control (cisplatin), it is verified that the distribution profile of the marking became very different from that seen with the negative control. The fact that immediately draws attention is the decrease in the percentage of cells in the G0/G1 phase (30.47%), which dropped by half compared to the marking of the negative control group.

But the distribution of cells in other phases was also affected, in this case both S and G2/M phases had an increase in cell numbers, which corresponded to approximately 27% and 24%, respectively. The percentage labelling in Sub-G1 almost doubled compared to that observed in the negative control. As can be seen in **Figure 12**, it is possible to see that exposure to AgNPs modified the cell cycle profile. The highest percentage of cells was found in G0/G1 (47.04%), while small percentages for S and G2/M phases (10.5 and 10.01%, respectively) were detected. A relevant finding is the high percentage of cells in Sub-G1 (32.09%), which is almost double that observed when cisplatin was used. When comparing the data from the negative control with those obtained after treatment with AgNPs, it is observed that the treatment led to a decrease of approximately 13% in the marking in the G0/G1 phase; 4.7% in phase S; and 4.1% in the G2/M phase. On the other hand, there is an increase of around 22% in the Sub-G1 phase.

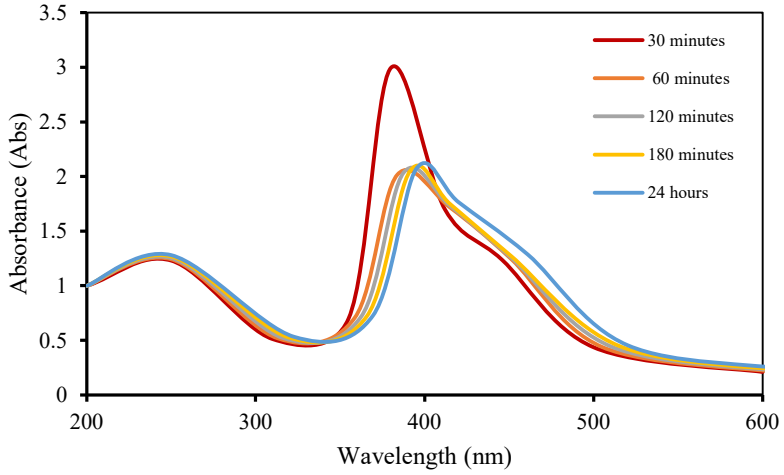

Figure 2: UV-Vis spectra of AgNP as a function of time

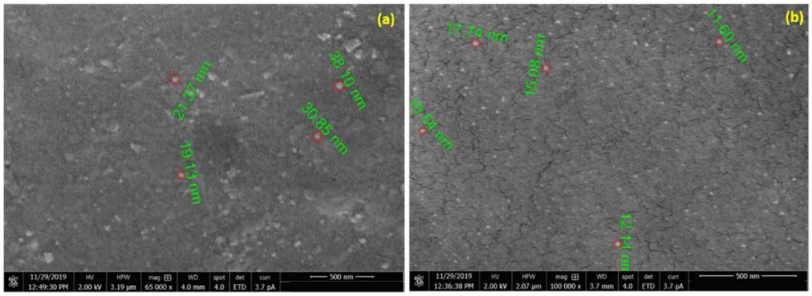

Figure 3: (a). Micrograph of the upper face of the AgNPs and (b) Micrograph of the cross section of the AgNPs surface

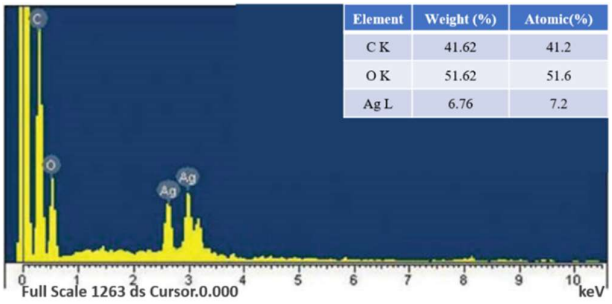

Figure 3c: EDX image of silver nanoparticles synthesized with the *P. ovata* leaf extract

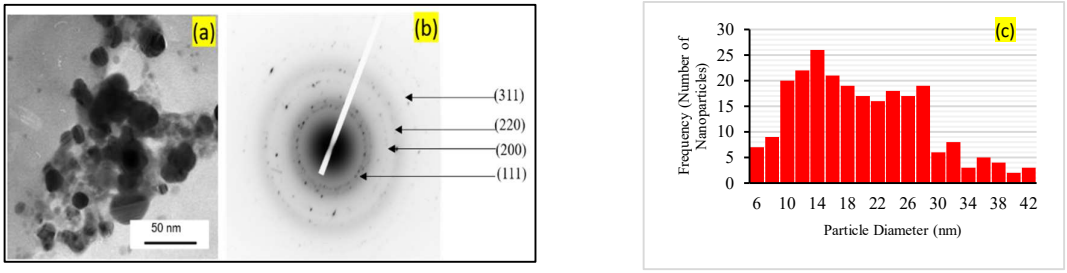

Figure 4: a) Silver Nanoparticles synthesized from *P. ovata* leaf extract b) SAED image of silver nanoparticles. (c) histogram of the Silver Nanoparticles

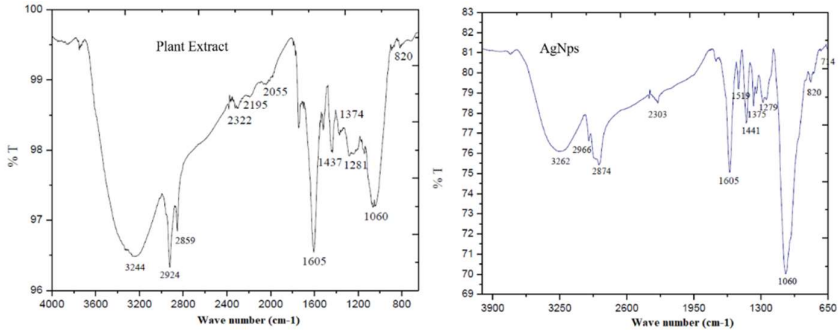

Figure 4: Analysis of peak positions obtained by infrared spectroscopy (FTIR) for Plant extract and AgNPs

Table 1: Data on mean diameter and zeta potential of the AgNPs obtained by dynamic light scattering (DLS). The values related to the average diameter are in nanometers (nm), and the zeta potential is in millivolts (mV)

Sample	Average Diameter (nm)	Zeta Potential (mV)
AgNPs	19.6 ± 9[b]	-29.7 ± 1.6[a]

Values represented by means of three independent experiments and their respective standard deviations. Letters [a] and [b] represent significant differences between samples ($p<0.05$)

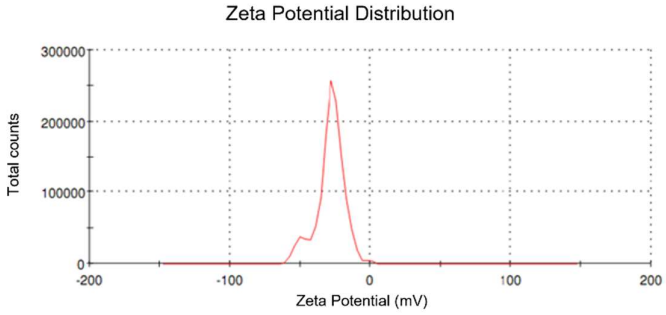

Figure 5: Zeta Potential image of AgNPs

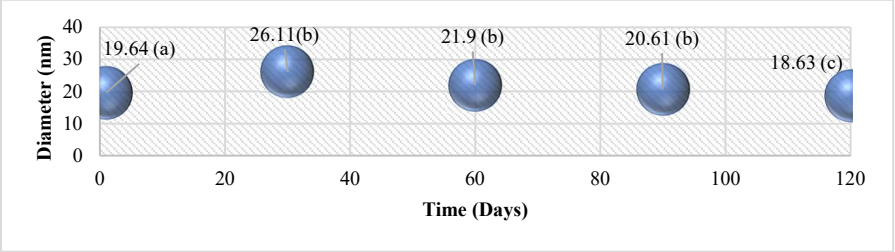

Figure 6: AgNPs stability assessment by the DLS technique over four months at 4°C. For stability analysis, mean diameters (nm) were evaluated over a period of four months. Letters (a), (b) and (c) represent significant difference p<0.05

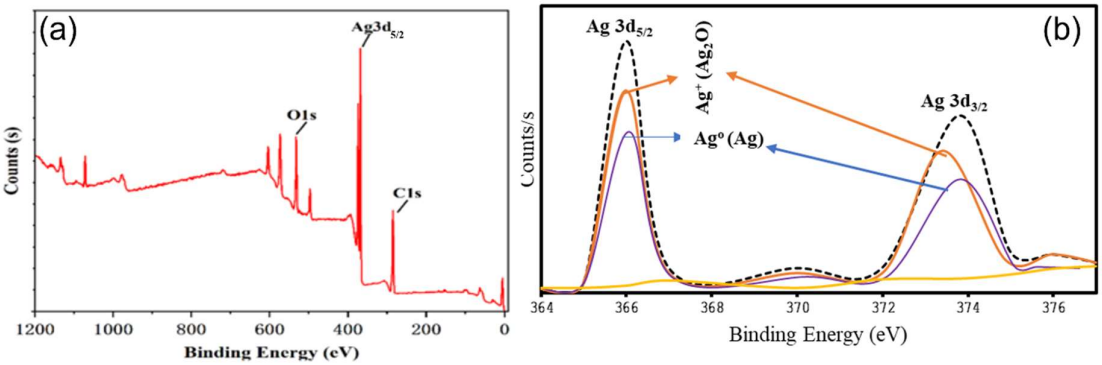

Figure 7: XPS spectra of silver nanoparticles synthesised from *P. ovata* leaf extract

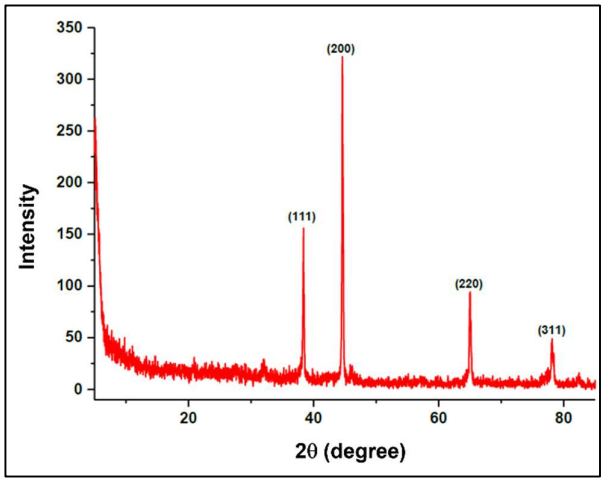

Figure 8: XRD image of Ag nanoparticles from *P. ovata* leaf extract

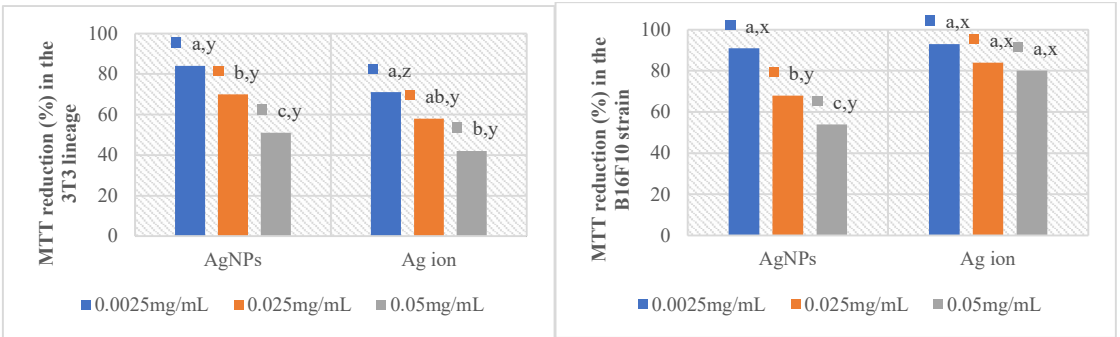

Figure 9: Influence of AgNPs and silver ion (from silver nitrate) on the MTT reduction capacity of 3T3 fibroblast cells (A) and B16F10 melanoma cells (B) after 24 hours of incubation. The histogram bars represent the relative percentage of MTT shrinkage. (*Values are represented as mean of three independent experiments ± standard deviation, letters a, b, c represents significant difference between different concentrations of the same sample; the letters x, y, z represents significant difference between equal concentrations of different samples (p<0.05)*)

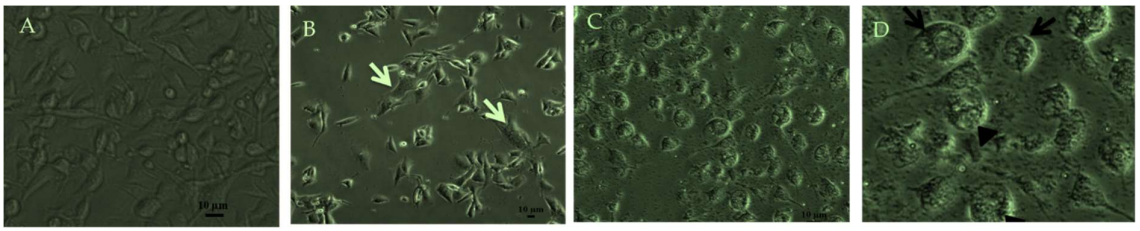

Figure 10: Photomicrographs of B16F10 cells visualized in an inverted phase-contrast microscope (magnified 400x) after 24 hours of incubation. (A) Negative control with cells of typical lineage (B) Positive control with cells treated with 0.3 µg/mL of cisplatin and some lamellipodia are highlighted (white arrow). (C) Cells treated with 0.5 mg/mL of AgNPs (D) Enlarged Fig C for observation of more details.

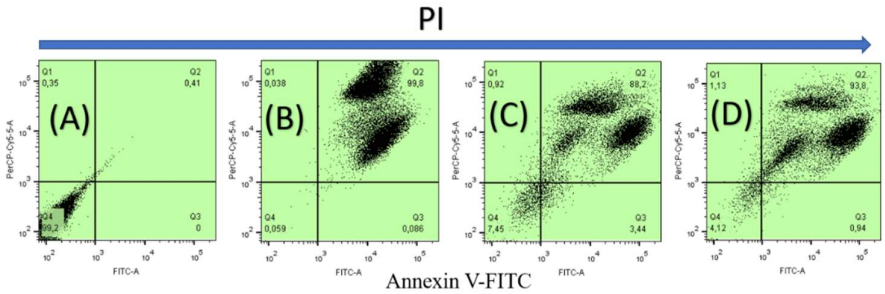

Figure 11: Analysis of labeling of B16F10 cells with annexin V and propidium iodide (PI) by flow cytometry

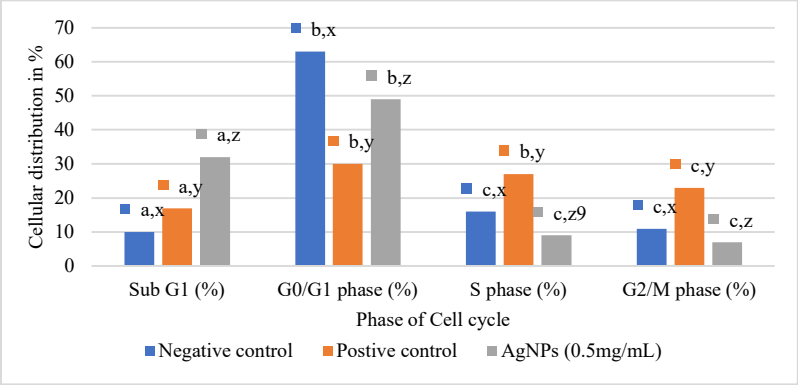

Figure 12: Cell cycle analysis by flow cytometry after 24 hours of incubation with cisplatin and nanoparticles in B16F10 melanoma cell line

4. DISCUSSION

As seen in the results section, it was possible to synthesize nanoparticles containing silver from *Pachygone ovata* (Poir.) Miers ex Hook.f. & Thomson leaf extract as reducing agent. The first results that confirmed this were those obtained through UV-visible light spectroscopy. The UV-Vis spectrum of AgNPs showed increased optical density (OD) in the region between 415-420 nm. This increase occurs because metallic nanoparticles exhibit a surface plasmonic resonance (SPR) due to the oscillation of electrons in metals after the incidence of light and is responsible for the appearance of bands or absorption peaks characteristic of each metal. In the case of silver nanoparticles, He *et al*. (2001) **[14]** indicated the range between 400 and 450 nm as the one in which signs of the presence of this metal can be observed. Other authors who synthesized silver nanoparticles containing extracts rich in terpenoids, carbohydrates and polyphenols also observed the increase

in OD in this region. However, the increase in OD observed in these studies was much more intense than that observed here. Continuing with the characterization, analyses were performed using SEM, EDX and DLS techniques, to unravel the size of the AgNPs. According to the images obtained by the SEM technique, the estimated average size of the AgNPs was 420 nm. These values were higher than those determined by the DLS technique (96 ± 13 nm). This type of behavior has already been reported by several authors such as Cheng *et al*. (2014) **[15]**. In most cases, the size determined by DLS was considered the most representative for nanoparticles, since it was determined when the particles were in suspension. Thus, it is assumed that the average size of the AgNPs evaluated in this work is 19 ± 6 nm.

The size of the nanoparticles interferes with the cytotoxicity and efficiency of the release of silver ions, some studies report that very small NPs have more significant cytotoxicity when compared to larger NPs, on the other hand, very large NPs may not be able to enter the cell. The ideal size for nanoparticles with *in vivo* applications is between 50-300 nm, as in this size range they do not quickly disperse through blood capillaries and do not attract macrophages from the reticuloendothelial system. Since the AgNPs in this study are within this size range, they are expected to be compatible with *in vivo* applications.

SEM -EDX techniques were used to evaluate the shape of the AgNPs, it is possible to observe in **Figure 7** that the AgNPs have a rounded shape. The rounded/spherical shape is familiar for most AgNPs synthesized via green synthesis involving polyphenols and carbohydrates as reducing agents. The homogeneity in the dispersion is related to the colloidal stability of AgNPs and the zeta potential. The zeta potential (ZP) is a measure of the surface charge of the particles, the zeta potential values greater than +30 mV and –30 mV are related to stable colloidal dispersions of nanoparticles. In this work, values of -27.59 mV were found for the fraction and -25.9 mV for the AgNPs, this means that the particles have a negative surface charge and are stable according to the values from Nayak *et al* (2015) **[16]**. The observed values are close to each other, indicating that the molecules responsible for the negative charge of the fraction are also present in the AgNPs, and may be responsible for their coating.

To identify and confirm which biomolecules were involved in the reduction of silver and stabilization of AgNPs, FTIR analyses were performed. This technique is adopted for researching functional groups in samples and is present in works that synthesize nanoparticles from seaweed extracts. In our

study, the spectrum of the n- hexane fraction was compared with the spectrum of AgNPs, according to **Figure 4**, we can visualize a graph with the main signals obtained. It is possible to observe a similarity between the signals obtained for the two samples.

Assays evaluating the ability to reduce MTT were essential for understanding the effects of nanoparticles on cell lines. In addition, they provide the basis for understanding the toxicity of the nanomaterial, which is highly relevant within biomedical research. In this study, we investigated the ability of AgNPs and silver to alter the ability of MTT reduction by cells of the 3T3 (fibroblasts) and B16F10 (melanoma) lineages. It is possible to observe from the results shown in **Figure 9A**, that all samples decreased the MTT reduction capacity of 3T3 cells. When the influence of the samples on the B16F10 strain is observed, it is verified that only with AgNPs a decrease in the reducing capacity was obtained ($p<0.05$). According to **Figure 9**, it is also possible to observe that silver alone decreased the MTT reducing capacity of normal cells (3T3). A similar effect has already been described by other authors who worked with non-tumor cells, Willcox, *et al*. (2014) **[17]** described that astrocytes had their ability to reduce MTT reduced by 60% due to the presence of silver in the culture medium. Tumor cells are also affected by the presence of silver, for example, 786-0 human renal adenocarcinoma cells had their ability to reduce MTT decreased by 40%, as well as the number of Jurkat T cells (leukemia) stained with trypan blue increased compared to the control group. The data presented here in **Figure 9** also lead to the observation that the B16F10 tumor cells did not have their ability to reduce MTT affected in the presence of silver, at least under the evaluated conditions, which gives evidence that silver cytotoxicity may be cell or that these cells are more resistant to the cytotoxic action of silver.

Unlike what happened with silver, the AgNPs synthesized here influenced the ability to reduce MTT, mainly in tumor cells. This shows that these agents were potentiated when they were unified in the form of nanoparticles. This feat was also observed by other authors who synthesized AgNPs by green methods, for example AgNPs synthesized with polysaccharide extracts from algae **[18]** also promoted a reduction in the ability to reduce MTT of tumor cells of the B16F10, 786-0 (renal adenocarcinoma) and HeLa (cervical cancer) cell lines, respectively. With the data presented here, it is still not possible to state whether the action of AgNPs on the ability of cells to reduce MTT is an action only of silver that reached the cytoplasm of cells, but there are no data with the B16F10 cell or with the alginate synthesized by the *P. ovata*. With the morphological analyses of

the cells, it was verified that the AgNPs altered more than the capacity of the B16F10 cells to reduce the MTT. It was found that the plates containing cells treated with AgNPs had more spaces without cells than the negative control group, indicating that there are fewer cells under the treatment conditions with AgNPs. In addition, the treated cells presented a globular aspect with granules in the cytoplasm. These findings indicate that the AgNPs provoked a disturbance in the cellular cytoskeleton, causing the change in the format as already observed in other studies. The cytoplasm granules come from cellular component degradation and may also represent an accumulation of AgNPs in the cytoplasm, as seen by other authors.

Together, the data discussed so far (MTT and morphology) provide evidence that AgNPs have an antiproliferative effect by inducing cell death. This led to the investigation of the probable antiproliferative mechanism. Therefore, labelling assays with annexin-V and propidium iodide and cell cycle analysis were performed. With the analysis of the distribution of B16F10 cells in the phases of the cell cycle, it was verified that after treatment with the nanoparticles there was an increase in the marking of propidium iodide in the sub-G1 phase and a decrease in marked cells in all other phases, which is in agreement with the annexin V-PI labelling data, and indicates increased cell death.

By analysing **Figure 11**, it is possible to see that most of the cells treated with cisplatin and AgNPs were doubly labelled for annexin-V-PI, even in the presence of the caspase inhibitor ZVAD, thus suggesting the occurrence of cell death by late apoptosis/necrosis. Foldbjerg *et al*. (2011) **[19]** synthesized AgNPs coated with polyvinylpyrrolidine and observed that their nanoparticles also led cells to late apoptosis/necrosis, in this case, in lung carcinoma cells (A549). And that would be its primary mechanism for inducing cell death. No studies state the exact mechanism of toxicity promoted by AgNPs; evidence of apoptosis, generation of ROS and DNA damage are the most commonly found findings in the literature **[20]**. This work's data indicate an antiproliferative potential by inducing late apoptosis/necrosis. However, it is expected to carry out future studies evaluating the mechanism of inducing cell death of AgNPs with 0.5mg/L concentration to fill this knowledge gap. And since it was not possible to prove whether the antiproliferative action of AgNPs occurred by releasing silver ions in the extracellular environment or with the penetration of AgNPs into the cell and subsequent release of ions, investigation studies about the mechanism of action and

penetration of AgNPs are also designed for the continuation of this work.

5. CONCLUSIONS

The results of this work show that it is possible to develop chemically functionalized silver nanoparticles using a "green" method that uses an n-hexane extract from the *Pachygone ovata* (Poir.) Miers ex Hook.f. & Thomson leaf extract as a reducer. Moreover, the synthesized AgNPs have well-defined characteristics, such as a diameter and shape compatible with *in vivo* applications, stability for 3 months. These AgNPs altered the ability to reduce MTT by 3T3 and B16F10 cells. AgNPs (0.5 mg/ml) induce cell death by late apoptosis/necrosis and cause increased labeling of B16F10 cells by propidium iodide in the sub-G1 phase.

6. CONFLICT OF INTEREST

The authors have no conflicts of interest regarding this investigation**.**

REFERENCES

[1] Krieghoff-Henning E, Folkerts J, Penzkofer A, Weg-Remers S. Cancer – an overview. *Med Monatsschr Pharm.* 2017;40(2):48-54.

[2] Ojima I. Recent advances in tumor-targeting chemotherapy drugs. *Cancer Drug Resistance.* 2021; 4(4):885-7. http://dx.doi.org/10.20517/cdr.2021.86.

[3] Dikshit PK, Kumar J, Das AK, Sadhu S, Sharma S, Singh S, Gupta PK, Kim BS. Green Synthesis of Metallic Nanoparticles: Applications and Limitations. *Catalysts*. 2021; 11(8):902..

[4] Li D, Liu Z, Yuan Y, Liu Y, Niu F. Green synthesis of gallic acid-coated silver nanoparticles with high antimicrobial activity and low cytotoxicity to normal cells. *Process Biochem.* 2015;50(3):357–366.

[5] Verónica Castro-Aceituno, Sungeun Ahn, Shakina Yesmin Simu, Priyanka Singh, Ramya Mathiyalagan, Hyun A. Lee, Deok Chun Yang, Anticancer activity of silver nanoparticles from Panax ginseng fresh leaves in human cancer cells, *Biomedicine & Pharmacotherapy*, 2016;84:158-165.

[6] Pradhan Arun, Sahoo Sameer, Satapathy Swapnashree, Pradhan Snehalata, Prusty Jyoti, Preetam Subham. Green synthesis of silver nanoparticles from various plant extracts and its applications: A mini review. *World Journal of Biology Pharmacy and Health Sciences*. 2022:11(01): 050–061

[7] Khan MS, Alomari A, Tabrez S, Hassan I, Wahab R, Bhat SA, Alafaleq NO, Altwaijry N, Shaik GM, Zaidi SK, Nouh W, Alokail MS, Ismael MA. Anticancer Potential of Biogenic Silver Nanoparticles: A Mechanistic Study. *Pharmaceutics*. 2021; 13(5):707. https://doi.org/10.3390/pharmaceutics13050707

[8] Bossy-Wetzel Ella, Green Douglas. Detection of Apoptosis by Annexin V Labeling. *Methods in enzymology.* 2000; 322: 15-18. 10.1016/S0076-6879(00)22004-1.

[9] Taware Ravindra, Abnave Prasad, Patil Deepak, Rajamohananan Pattuparambil, Raja Remya, Shankar Gowri, Kundu Gopal, Kharat Maheshkumar, Pai Kalpana, Ahmad Absar. Trichothecin from Endophytic Fungus Trichothecium sp. and its Antican-cer Effect on Murine Melanoma and Breast Cancer Cell Lines. *Current Biochemical Engineering*. 2015: 2:73-80.

[10] Erjaee, H.; Rajaian, H.; Nazifi, S. Synthesis and characterization of novel silver nanoparticles using Chamaemelum nobile extract for antibacterial application. *Advances in Natural Sciences: Nanoscience and Nanotechnology*. 2017;8:025004 (9pp), https://doi.org/10.1088/2043-6254/aa690b

[11] Hassanein Ahmed, Hussein Raghda, Farghali Ahmad, Ibraheem Ibraheem. Biosynthesis of silver nanoparticles by using of the marine alga Gracilaria parvispora and its antagonistic efficacy against some common skin infecting pathogens. *Australian Journal of Basic and Applied Sciences*. 2017: 11:219-227.

[12] Ramachandran, Kumarasamy, Kalpana, Duraisamy, Sathishkumar Y, Lee Y, Ravichandran K, Kumar G. A facile green synthesis of silver nanoparticles using *P.betel* biomass and its catalytic activity toward sensitive and selective nitrite detection. *Journal of Industrial and Engineering Chemistry*. 2016; 35: 29-35.

[13] Gupta D, Chauhan P. Green Synthesis of Silver Nanoparticles Involving Extract of Plants of Different Taxonomic Groups. *Journal of Nanomedicine Research*. 2017;5(2):11–12.

[14] He S, Yao J, Jiang P, Shi D, Zhang H, Xie S, Pang S, Gao, H. Formation of silver nanoparticles and self-assembled two-dimensional ordered superlattice. *Langmuir*, 2001:17 (5):1571–1575.

[15] Cheng K, Hung Y, Chen C, Liu C, Young J. Green synthesis of chondroitin sulfate-capped silver nanoparticles: Characterization and surface modification. *Carbohydrate Polymers*, 2014: 110: 195–202.

[16] Nayak D, Pradhan S, Ashe S, Rauta PR, Nayak B. Biologically synthesised silver nanoparticles from three diverse family of plant extracts and their anticancer activity against epidermoid A431 carcinoma. *Journal of Colloid and Interface Science*, 2015: 457: 329–338,

[17] Willcox JM, Summerlee AJS, Relaxin Protects Astrocytes from Hypoxia *In Vitro*. *PLoS ONE* 2014; 9(3): e90864. https://doi.org/10.1371/journal.pone.0090864.

[18] El-Rafie, Hanaa, El-Rafie, M. Green synthesis of silver nanoparticles using polysaccharides extracted from marine macro algae. *Carbohydrate polymers*. 2013; 96: 403-410.

[19] Foldbjerg R, Dang DA, Autrup H. Cytotoxicity and genotoxicity of silver nanoparticles in the human lung cancer cell line, A549. *Archives of Toxicology*, 2011; 85 (7):743–750

[20] Hamedi S. Shojaosadati SA, Mohammadi A. Evaluation of the catalytic, antibacterial and anti-biofilm activities of the Convolvulus arvensis extract functionalized silver nanoparticles, *Journal of Photochemistry and Photobiology B: Biology,* 2017: 167: 36-44.